

Convolutional Monge Mapping between EEG Datasets to Support Independent Component Labeling

Austin Meek¹, Carlos H. Mendoza-Cardenas², and Austin J. Brockmeier³

Abstract—EEG recordings contain rich information about neural activity but are subject to artifacts, noise, and superficial differences due to sensors, amplifiers, and filtering. Independent component analysis and automatic labeling of independent components (ICs) enable artifact removal in EEG pipelines. Convolutional Monge Mapping Normalization (CMMN) is a recent tool used to achieve spectral conformity of EEG signals, which was shown to improve deep neural network approaches for sleep staging. Here we propose a novel extension of the CMMN method with two alternative approaches to computing the source reference spectrum the target signals are mapped to: (1) channel-averaged and l_1 -normalized barycenter, and (2) a subject-to-subject mapping that finds the source subject with the closest spectrum to the target subject. Notably, our extension yields space-time separable filters that can be used to map between datasets with different numbers of EEG channels. We apply these filters in an IC classification task, and show significant improvement in recognizing brain versus non-brain ICs.

Clinical relevance—EEG recordings are used in the diagnosis and monitoring of multiple neuropathologies, including epilepsy and psychosis. While EEG analysis can benefit from automating artifact removal through independent component analysis and labeling, differences in recording equipment and context (the presence of noise from electrical wiring and other devices) may impact the performance of machine learning models, but these differences can be minimized by appropriate spectral normalization through filtering.

I. INTRODUCTION

In machine learning, out-of-distribution data (data from different domains) can deteriorate performance of models, especially when trained on limited data. The model may be sensitive to differences in the data distribution that are not actually relevant to the task. In the context of biomedical data, domains may correspond to different equipment, recording settings, or the population of individuals. In the context of EEG, differences in set-up (electrodes, amplifiers, analog and digital filters, power line noise) can create stark changes in the spectral content of recordings. One method to address this problem is the Convolutional Monge Mapping Normalization (CMMN) approach for spectral normalization based on optimal transport [1], which optimizes a linear filter for each subject and channel such that after filtering all subjects have the same spectrum for that channel, which

is the barycenter of the channel’s spectra for all training subjects. Originally, CMMN was applied to sleep staging with deep neural networks.

In this work, we extend it to the case of automatically labeling independent components, such as the popular ICLabel classifier [2], which can support automatic EEG artifact removal and denoising. In comparison to the ICLabel classifier, which uses a neural network model with scalp map and spectral features (including the autocorrelation sequence), and was trained on an extensive dataset [3], we consider custom classifiers trained on a much smaller dataset collected in the US [4] using only time-series features extracted from each independent component [5]—that is, without any spatial information. We then test on an another independent dataset [6], collected in Europe. These two datasets were used in a prior work on IC classification [7], and are now both available on OpenNeuro [8], [9]. Because these datasets have expert-labeled ICs, we avoid filtering each channel with a different filter, which would change each IC differently; instead, we find a single CMMN filter for each subject that is applied to all channels. This channel-averaged CMMN filter is based on matching the channel-averaged spectrum of each test subject to either the barycenter of the channel-averaged spectra from the training set or the nearest spectrum in the training set in terms of the optimal transport distance. With a shared single temporal filter across channels, the filtering can be applied before or after the spatial filtering achieved by ICA’s demixing matrix. That is, the joint filtering is separable.

Crucially, the use of the channel-averaging enables the application of CMMN to target domains with a differing number of channels. Here, the source (train) and target (test) datasets have 134–235 channels and 64 channels, respectively.

This extension of the CMMN methodology achieves domain adaptation between two datasets with the pre-trained classifiers such that their performance (the subject averaged F1 score for the brain class is 0.91) exceeds the performance of the ICLabel (0.88).

II. METHODOLOGY

We first detail the background of convolutional Monge mapping normalization [1] that was not wholly contained in that work. We then detail the proposed additions.

A. Background

The CMMN methodology enables domain adaptation between different neural signals [1] by mapping the spectra of

¹A. Meek is affiliated with the Department of Computer and Information Sciences, University of Delaware ajmeek@udel.edu

²C. H. Mendoza-Cardenas is an Applied Scientist at Twitch Interactive Inc., San Francisco, California, USA

³A. J. Brockmeier is affiliated with the Department of Electrical and Computer Engineering, Department of Computer and Information Sciences, University of Delaware, Newark, Delaware, USA ajbrock@udel.edu

The source code for our implementation and experiments is publicly available at <https://github.com/cniel-ud/ICWaves>.

the target subjects to the barycenter of the source subjects via a linear filter that achieves the optimal transport (under an ℓ_2 -metric) under zero-mean stationary Gaussian discrete-time processes. This follows from the fact that the Wasserstein-2 distance between Gaussian distributions has a closed form [10], [11] known as the Bures-Wasserstein distance or Fréchet distance, expressed in terms of the means $\mathbf{m}^S, \mathbf{m}^T$ and covariance matrices Σ^S, Σ^T , as

$$W_2(\mathcal{N}(\mathbf{m}^S, \Sigma^S), \mathcal{N}(\mathbf{m}^T, \Sigma^T)) = \sqrt{\|\mathbf{m}^S - \mathbf{m}^T\|_2^2 + \text{tr}(\Sigma^S + \Sigma^T - (\Sigma^{S\frac{1}{2}} \Sigma^T \Sigma^{S\frac{1}{2}})^{\frac{1}{2}})}, \quad (1)$$

where the second term in the square root is the squared Bures distance. Under the stationarity assumption, a discrete-time zero-mean Gaussian process is completely described by its auto-covariance matrix, which is a symmetric and Toeplitz matrix formed from the auto-correlation sequence $r[k] = \mathbb{E}[x[n]x[n+k]]$. Assuming $r[\tau]$ decays for increasing lags and taking a sufficiently large lag (or applying a windowing function to the auto-correlation sequence as in the Blackman-Tukey method), and optionally padding with Q zeros, the auto-correlation sequence can be formed into an $N \times N$ circulant matrix (necessarily Toeplitz and still symmetric) where

$$\mathbf{r} = [r[0], r[1], \dots, r[K-1], \underbrace{0, \dots, 0}_Q, r[-K+1], \dots, r[-1]] \quad (2)$$

is the first column. Let Σ_r denote the resulting $N \times N$ circulant matrix, with $N = 2K - 1 + Q$. Then, the discrete Fourier transform (DFT) matrix $\mathbf{F} = [e^{-i\frac{2\pi kn}{N}}]_{k=1, n=1}^{N, N}$ diagonalizes it, $\mathbf{F}\Sigma_r\mathbf{F}^H = \text{diag}(\lambda_r)$, where \mathbf{F}^H denotes the Hermitian transpose of \mathbf{F} and $i = \sqrt{-1}$. The resulting diagonal

$$\lambda_r = \text{diag}(\mathbf{F}\Sigma_r\mathbf{F}^H) = \mathbf{F}\mathbf{r} \quad (3)$$

corresponds to an statistical estimate of the power spectral density (PSD). In contrast, a finite-window periodogram estimate of the PSD is

$$\lambda = \mathbb{E}[(\mathbf{F}\mathbf{x})^{\odot 2}] = \mathbb{E}[\text{diag}(\mathbf{F}\mathbf{x}\mathbf{x}^H\mathbf{F}^H)] = \text{diag}(\mathbf{F}\mathbb{E}[\mathbf{x}\mathbf{x}^H]\mathbf{F}^H) = \text{diag}(\mathbf{F}\Sigma\mathbf{F}^H), \quad (4)$$

where \mathbf{x} is a window of length N from the process and \odot denotes elementwise power. Note that clearly λ and $\Sigma = \mathbb{E}[\mathbf{x}\mathbf{x}^H]$ are non-negative and positive semidefinite, respectively. Σ will only be circulant under the assumption of periodic discrete-time signals such that $\Sigma = \Sigma_r$ and $\lambda = \lambda_r$; otherwise, $\mathbf{F}\Sigma\mathbf{F}^H$ will not be strictly diagonal. The Wiener-Khinchin theorem, equating the Fourier transform of the autocorrelation with the power spectral density, only holds for infinitely auto-correlation sequences. Truncating the auto-correlation sequence, without proper choice of a windowing function, can lead to a circulant matrix Σ_r which is not positive semidefinite, yielding negative values in the spectrum. The truncation corresponds to a rectangular window whose Fourier transform is a sinc function, which takes positive and negative values. Multiplication in time-domain causes convolution in the frequency domain and the

result may be negative. Using a windowing function whose Fourier transform is strictly positive, such as the Barlett (triangular), Parzen, or Gaussian, will ensure a non-negative spectrum. In fact, the finite-window periodogram estimate (4) uses a Barlett window.

The squared Wasserstein-2 distance between two discrete-time, zero-mean stationary Gaussian random processes with auto-covariance Σ^S and Σ^T , which are circulant, is

$$W_2(\mathcal{N}(\mathbf{0}, \Sigma^S), \mathcal{N}(\mathbf{0}, \Sigma^T)) = \|\lambda^{S\odot\frac{1}{2}} - \lambda^{T\odot\frac{1}{2}}\|_2, \quad (5)$$

using the fact that if two matrices share the same basis, then the Bures distance is the Euclidean distance between the square root of their spectra. This can be seen directly by substituting $\Sigma^S = \mathbf{F}^H \text{diag}(\lambda^S) \mathbf{F}$ and $\Sigma^T = \mathbf{F}^H \text{diag}(\lambda^T) \mathbf{F}$ into the squared Bures distance and using $\mathbf{F}^H \mathbf{F} = \mathbf{I}$:

$$\begin{aligned} & \text{tr}(\Sigma^S + \Sigma^T - (\Sigma^{S\frac{1}{2}} \Sigma^T \Sigma^{S\frac{1}{2}})^{\frac{1}{2}}) \\ &= \text{tr}(\mathbf{F}^H \text{diag}(\lambda^S) \mathbf{F} + \mathbf{F}^H \text{diag}(\lambda^T) \mathbf{F} \\ &\quad - (\mathbf{F}^H \text{diag}(\lambda^{S\odot\frac{1}{2}}) \text{diag}(\lambda^T) \text{diag}(\lambda^{S\odot\frac{1}{2}}) \mathbf{F})^{\frac{1}{2}}) \\ &= \text{tr}(\text{diag}(\lambda^S) + \text{diag}(\lambda^T) - (\mathbf{F}^H \text{diag}(\lambda^S \odot \lambda^T) \mathbf{F})^{\frac{1}{2}}) \\ &= \text{tr}(\text{diag}(\lambda^S) + \text{diag}(\lambda^T) - \mathbf{F}^H \text{diag}(\lambda^{S\frac{1}{2}} \odot \lambda^{T\frac{1}{2}}) \mathbf{F}) \\ &= \sum_{n=0}^{N-1} \lambda^S[n] + \lambda^T[n] - \sqrt{\lambda^S[n] \lambda^T[n]} \\ &= \|\lambda^{S\odot\frac{1}{2}} - \lambda^{T\odot\frac{1}{2}}\|_2^2, \end{aligned} \quad (6)$$

where \odot also denotes the elementwise (Hadamard) product.

The Bures-Wasserstein barycenter, which is the Gaussian special case of the Wasserstein-2 barycenter [12], [13], is the covariance matrix Σ_S (in the set of positive semidefinite matrices \mathcal{S}_N) that minimizes the sum of squared Wasserstein-2 distances to a set of zero-mean Gaussian distributions described by covariance matrices $\{\Sigma_i^S\}_{i=1}^I$:

$$\Sigma_S = \arg \min_{\Sigma \in \mathcal{S}_N} \sum_{i=1}^I \frac{1}{I} W_2^2(\mathcal{N}(\mathbf{0}, \Sigma), \mathcal{N}(\mathbf{0}, \Sigma_i^S)), \quad (7)$$

In the case, that all the covariance matrices are circulant and positive semidefinite, it is straightforward to show that $\Sigma_S = \mathbf{F}^H \text{diag}(\bar{\lambda}_S) \mathbf{F}$, where $\bar{\lambda}_S = (\frac{1}{I} \sum_i \lambda_i^{S\odot\frac{1}{2}})^{\odot 2}$. Using (5),

$$\sum_{i=1}^I \frac{1}{I} W_2^2(\mathcal{N}(\mathbf{0}, \Sigma), \mathcal{N}(\mathbf{0}, \Sigma_i^S)) = \sum_{i=1}^I \frac{1}{I} \|\lambda^{\odot\frac{1}{2}} - \lambda_i^{S\odot\frac{1}{2}}\|_2^2. \quad (8)$$

Taking the derivative with respect to $\lambda^{\odot\frac{1}{2}}$ yields $\lambda^{\odot\frac{1}{2}} = \frac{1}{I} \sum_i \lambda_i^{S\odot\frac{1}{2}}$.

Consider a stationary target signal $x[n]$ with PSD $\lambda^T = \mathbb{E}[|\mathbf{F}\mathbf{x}|^{\odot 2}]$ that is convolved with the filter impulse response $h[n]$ (frequency response \mathbf{H}), yielding the signal $y[n] = (h * x)[n]$. Then under the stationarity assumption, the PSD of $y[n]$ is

$$\lambda^y = \mathbb{E}[|\mathbf{F}\mathbf{y}|^{\odot 2}] = \mathbb{E}[|(\mathbf{F}\mathbf{x}) \odot \mathbf{H}|^{\odot 2}] \quad (9)$$

$$= \mathbb{E}[|\mathbf{F}\mathbf{x}|^{\odot 2} \odot |\mathbf{H}|^{\odot 2}] = |\mathbf{H}|^{\odot 2} \odot \mathbb{E}[|\mathbf{F}\mathbf{x}|^{\odot 2}] \quad (10)$$

$$= |\mathbf{H}|^{\odot 2} \odot \lambda^T, \quad (11)$$

where \mathbf{H} is the discrete Fourier transform of the filter. Assuming $x[n]$ is also zero-mean and a Gaussian process $\mathbf{x} \sim \mathcal{N}(\mathbf{0}, \Sigma^T)$, then $y[n]$ has a circulant auto-covariance matrix $\Sigma^y = \mathbf{F} \text{diag}(|\mathbf{H}|^{\odot 2} \odot \boldsymbol{\lambda}^T) \mathbf{F}^H$. The Wasserstein-2 distance between a source process (possibly the barycenter) and the filtered target process is then

$$W_2(\mathcal{N}(\mathbf{0}, \Sigma^S), \mathcal{N}(\mathbf{0}, \Sigma^y)) = \|\boldsymbol{\lambda}^{S \odot \frac{1}{2}} - |\mathbf{H}| \odot \boldsymbol{\lambda}^{T \odot \frac{1}{2}}\|_2^2. \quad (12)$$

Clearly, the distance is zero for any filter $h[n]$ such that

$$|\mathbf{H}| = \boldsymbol{\lambda}^{S \odot \frac{1}{2}} \odot \boldsymbol{\lambda}^{T \odot -\frac{1}{2}} \in \mathbb{R}_{\geq 0}^N, \quad (13)$$

i.e., where the magnitude of the frequency response is the square-root of the power spectral densities $|H[n]| = \sqrt{\frac{\lambda^S[n]}{\lambda^T[n]}}$, $n \in \{0, \dots, N-1\}$.

B. Proposed Methodology

We extend this methodology in two key ways: we propose to use channel-averaged PSDs yielding a single filter per subject and a subject-to-subject mapping scheme. A key benefit of using a single filter per subject is that it enables adapting between EEG datasets with a variable number of channels. We also propose to use ℓ_1 -normalization of spectra for invariance to signal scale, which may occur due to impedance differences due to electrodes or scalp contact or differences in the electronic systems (amplifiers and filtering) or digital filtering.

The ℓ_1 -normalized PSD is a probability mass function (PMF)—non-negative and sums to 1. Let $\tilde{\boldsymbol{\lambda}}^S = \frac{\boldsymbol{\lambda}^S}{\|\boldsymbol{\lambda}^S\|_1}$, this corresponds to the circulant matrix $\boldsymbol{\rho}^S = \frac{\Sigma^S}{\text{tr}(\Sigma^S)}$, and likewise for the target. Then, the Wasserstein-2 distance between two discrete-time zero-mean variance-normalized stationary Gaussian random processes is

$$W_2(\mathcal{N}(\mathbf{0}, \boldsymbol{\rho}^S), \mathcal{N}(\mathbf{0}, \boldsymbol{\rho}^T)) = \|\tilde{\boldsymbol{\lambda}}^{S \odot \frac{1}{2}} - \tilde{\boldsymbol{\lambda}}^{T \odot \frac{1}{2}}\|_2 \quad (14)$$

$$= \sqrt{2 - 2\langle \tilde{\boldsymbol{\lambda}}^{S \odot \frac{1}{2}}, \tilde{\boldsymbol{\lambda}}^{T \odot \frac{1}{2}} \rangle} \quad (15)$$

$$= \sqrt{2} \sqrt{1 - \langle \tilde{\boldsymbol{\lambda}}^{S \odot \frac{1}{2}}, \tilde{\boldsymbol{\lambda}}^{T \odot \frac{1}{2}} \rangle} = \sqrt{2} d_{\text{He}}(\tilde{\boldsymbol{\lambda}}^S, \tilde{\boldsymbol{\lambda}}^T), \quad (16)$$

where d_{He} denotes the Hellinger distance, which is applicable since the ℓ_1 -normalized PSDs reside on the probability simplex $\Delta^N = \{\tilde{\boldsymbol{\lambda}} \in \mathbb{R}_{\geq 0}^N : \sum_{n=0}^{N-1} \tilde{\lambda}[n] = 1\}$. The use of Hellinger distance compared to Bures-Wasserstein distance means that signals are compared in terms of their spectral shape, without regard to their variance.

Given this background, we now proceed to consider access to data (multichannel EEG) from I subjects in the source domain and one or more target subjects. We apply CMMN to transform the target EEGs to the source domain and apply classifiers trained on the source domain to the transformed target data. Let $x_c[n]$ denote the c -th channel of the target signal, $c \in \{1, \dots, C^T\}$. The CMMN transformation is a linear filtering of $x_c[n]$:

$$y_c[n] = (h * x_c)[n], \quad c \in \{1, \dots, C^T\}, \quad (17)$$

where $h[n]$ is the normalizing CMMN filter, and $y_c[n]$ is the transformed signal that will have a source-like spectrum (the

channel-averaged PSDs will match). The estimation of the normalizing CMMN filter is a three-step process that uses a reference spectrum (computed in the second step) that is either a **Barycenter** from the source or the normalized PSD of a source subject via the subject-to-subject (**Subj-to-subj**) assignment:

- 1) Power spectral density calculation
- 2a) Barycenter calculation
- 2b) Minimization of the Hellinger distance between target signals and source signals for the **Subj-to-subj** mapping scheme
- 3) Calculation of the normalizing filters

Step 1 PSD calculation. As in [1], we use the Welch periodogram method [14], which takes averages of the squared FFT from possibly overlapping windows, to calculate PSDs for each subject, as implemented by the SciPy library [15]. For real-valued signals, the spectra will be conjugate symmetric for positive and negative frequencies. In this case, $\mathbf{p} \in \mathbb{R}_{\geq 0}^P$ denotes the PSD for P non-negative frequencies (for zero-mean signals the DC component should be zero but is retained). For K equal-sized windows of length M , $\{\mathbf{x}_k\}_{k=1}^K = \mathcal{X} \subset \mathbb{R}^M$ with windowing function \mathbf{w} , the power spectral density estimate is

$$\mathbf{p} = \frac{1}{|\mathcal{X}|} \sum_{\mathbf{x} \in \mathcal{X}} |\text{RFFT}(\mathbf{w} \odot \mathbf{x})|^{\odot 2} \in \mathbb{R}_{\geq 0}^P, \quad (18)$$

where RFFT denotes the FFT operation for real-valued signals and returns the density estimate only for non-negative frequencies, $P = \text{nfft}/2 + 1$ is the number of non-negative frequencies, and $N = \text{nfft}$ is the length of the windows after zero-padding, assumed to be even.

For a subject with C channels, the matrix of PSDs is $\mathbf{P} = [\mathbf{p}_1, \dots, \mathbf{p}_C]^T \in \mathbb{R}^{C \times P}$. Unlike the original CMMN, which used different filters for each channel, we propose to compute a channel-averaged PSD as $\bar{\mathbf{p}} = \frac{1}{C} \sum_{c=1}^C \mathbf{p}_c$.

Step 2a Barycenter calculation. We compute a barycenter for the source subjects only, this serves as the template for mapping the target subjects. The barycenter for I source subjects $\bar{\mathbf{p}}_1^S, \dots, \bar{\mathbf{p}}_I^S$ channel-averaged PSDs is defined as

$$\bar{\mathbf{p}}_S = \frac{1}{I} \sum_{i=1}^I \bar{\mathbf{p}}_i^S. \quad (19)$$

Additionally, for robustness against differing scales we propose an option for calculating a normalized barycenter for the source subjects, where each source subject PSD is normalized, as

$$\tilde{\mathbf{p}}_S = \frac{1}{I} \sum_{i=1}^I \frac{\bar{\mathbf{p}}_i^S}{\|\bar{\mathbf{p}}_i^S\|_1} = \frac{1}{I} \sum_{i=1}^I \tilde{\mathbf{p}}_i^S, \quad \text{where } \tilde{\mathbf{p}}_i^S = \frac{\bar{\mathbf{p}}_i^S}{\|\bar{\mathbf{p}}_i^S\|_1}. \quad (20)$$

This ensures that each subject contributes equally to the average. Note that as the units of PSD are squared, outliers without normalization can influence the average. However, we avoided channel-wise normalization because that could change the contribution of individual channels, but this option could also be explored.

Step 2b Subject-to-subject mapping scheme for post-hoc alignment. Our proposed alternative to the barycenter mapping scheme associates a given target subject to the closest source subject with respect to the Wasserstein distance between variance-normalized zero-mean stationary Gaussian processes, which as stated is proportional to the Hellinger distance. Let $\tilde{\mathbf{p}}^T = \frac{\tilde{\mathbf{p}}^T}{\|\tilde{\mathbf{p}}^T\|_1}$ denote the ℓ_1 -normalized channel-averaged PSD for a particular target subject. The channel-averaged PSD of best matched source subject $\tilde{\mathbf{p}}_*^S$ is

$$\tilde{\mathbf{p}}_*^S = \tilde{\mathbf{p}}_{i^*}^S, \quad i^* = \arg \min_{i \in \{1, \dots, I\}} d_{\text{He}}(\tilde{\mathbf{p}}_i^S, \tilde{\mathbf{p}}^T), \quad (21)$$

where the Hellinger distance between two normalized PSDs $\tilde{\mathbf{p}}^S, \tilde{\mathbf{p}}^T \in \Delta^P \subset [0, 1]^P$, where $\Delta^P = \{\tilde{\mathbf{p}} \in \mathbb{R}_{\geq 0}^P : \sum_{n=0}^{P-1} \tilde{p}[n] = 1\}$ denotes the probability simplex, is

$$d_{\text{He}}(\tilde{\mathbf{p}}^S, \tilde{\mathbf{p}}^T) = \frac{1}{\sqrt{2}} \|\tilde{\mathbf{p}}^{S \odot \frac{1}{2}} - \tilde{\mathbf{p}}^{T \odot \frac{1}{2}}\|_2 \quad (22)$$

$$= \frac{1}{\sqrt{2}} \sqrt{\sum_{n=0}^{P-1} \left(\sqrt{\tilde{p}^S[n]} - \sqrt{\tilde{p}^T[n]} \right)^2}. \quad (23)$$

Step 3 Normalizing filter. We define a real-valued, zero-phase linear filter with impulse response $h[n]$ and frequency response \mathbf{H} . This filter solves the optimal transport problem for both the barycenter and subject-to-subject formulations, and its frequency response is given by the square root of the ratio of the channel-averaged PSDs [16]:

$$\mathbf{h} = \text{IRFFT}_M(\mathbf{H}), \quad (24)$$

$$\mathbf{H} = \tilde{\mathbf{p}}^{T \odot -\frac{1}{2}} \odot \tilde{\mathbf{p}}^{S \odot \frac{1}{2}}, \quad (25)$$

$$H[n] = \frac{\sqrt{\tilde{p}^S[n]}}{\sqrt{\tilde{p}^T[n]}}, \quad n \in \{0, \dots, P-1\}, \quad (26)$$

where IRFFT_M is the inverse FFT for real-valued signals that operates on the non-negative frequencies. As discussed in Section II-A, by equalizing the channel-average PSD, this filter solves the optimal transport problem between zero-mean Gaussian distributions with circulant covariance matrices that commute and are diagonalized by the discrete-time Fourier transform. For this filter, the source PSD $\tilde{\mathbf{p}}^S$ can be either the barycenter of the source dataset $\tilde{\mathbf{p}}_S$ (19), its ℓ_1 -normalized version $\tilde{\mathbf{p}}_S$ (20), or the closest matching source signal $\tilde{\mathbf{p}}_*^S$ (21).

C. Application of CMMN to pre-trained IC classifiers

While the proposed methodology is general and could be applied to normalize any target dataset for classifiers pre-trained on a source dataset, we focus on classifiers for automatically labeling independent components of EEG into brain and other classes [17], [7], [2]. In particular, we build on prior work [5], applying the CMMN approach to different types of classifiers (trained without CMMN):

- 1) Random forest classifiers that use features from the PSD and autocorrelation sequence of the independent components, as in the MNE-ICLabel implementation [18], a Python port of ICLabel [2].

- 2) Random forest classifiers that use the bag-of-waveforms (BoWaves) features [5], which are built on the occurrence of a dictionary of waveforms learned through a shift invariant k -means algorithm [19].

III. EXPERIMENTS AND RESULTS

A. Data

We use two datasets for this domain adaptation study, the *Imagined Emotion* dataset from [8] as the source dataset and the *Cue* dataset from [6] as the target dataset. Both datasets include manually labeled independent components (ICs). We hereafter refer to the *Imagined Emotion* dataset as simply the *Emotion* dataset.

The *Emotion* dataset has data from 32 subjects (13 male and 19 female, with an age mean and standard deviation of 25.5 ± 5 years). The EEG data has 180-232 channels and sampled at 256 Hz with durations ranging from 54 to 136 minutes. Channels with abnormal activity before performing ICA were discarded, leaving 134–235 channels per subject. This dataset was collected in the US, leaving a characteristic 60 Hz spike from AC electrical wiring as seen in Fig. 1. The dataset includes 935 expert-labeled ICs in three categories: brain (570), muscle (306), and eye (59). We used 27 subjects for training and 7 for testing. The training set contains 5,786 total ICs.

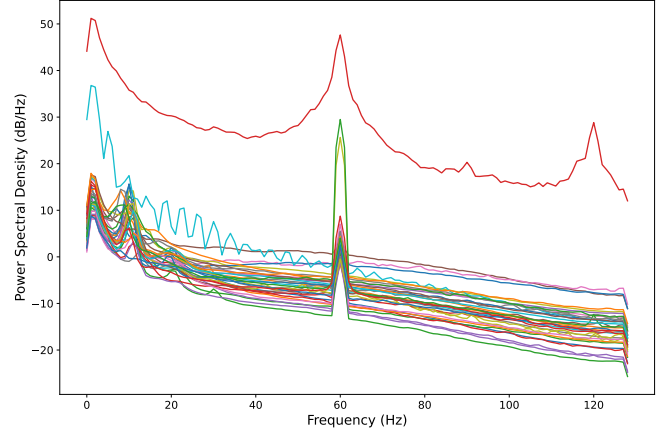


Fig. 1. Channel-averaged power spectral densities for each subject in the *Emotion* (source) dataset. Notice that some subjects are outliers in terms of overall amplitude.

The *Cue* dataset has data from 12 subjects (10 male, 2 female, with an age range of 21 to 25 years), using 64 channels during data collection. This dataset's recordings were 56 to 66 minutes long and were collected at 500 Hz, which we down-sampled to 256 Hz before performing domain adaptation. This dataset was collected in Europe, leaving a characteristic 50 Hz spike as seen in Fig. 3. Expert annotations are available for 389 ICs: brain (261), muscle (102), eye (22), and heart (4). This dataset serves as the target for cross-dataset evaluation, testing generalization of the classifiers trained on the *Emotion* training data.

Note that in comparison to the experiments in the original CMMN paper [1], our data contains different numbers of

channels (134–235 vs. 64). Therefore, the use of channel-averaged PSDs for CMMN is essential. For further details on both datasets, please refer to [8], [6].

B. IC classifiers

We trained multi-class classifiers using each feature set (BoWaves or PSD+Autocorrelation) on the subset of 27 subjects from *Emotion* dataset, with hyperparameters selected by leave-one-subject-out (LOO) cross-validation accuracy. The classifier is trained on segments of length l_{train} (a hyperparameter), and validated (using the F1 score on the brain class) on segments of length $l_{\text{val}} \in \{5, 50\}$ minutes, with $l_{\text{train}} \leq l_{\text{val}}$. Given the best LOO hyperparameters, a new model is trained on the entire training set of 27 subjects. Here we report test results on segments of length equal to the validation segment length, from a disjoint test set of 7 source *Emotion* subjects and all the target subjects in the *Cue* dataset.

We benchmark our method against ICLabel [2]. As a model trained on an extensive dataset of expert- and crowd-labeled ICs, ICLabel serves as a strong baseline that can be applied to both the source and target datasets without our proposed CMMN. Importantly, ICLabel uses the spatial information in the form of the mixing vector corresponding to the topographic map for each IC, which is not included in the BoWaves or the PSD and Autocorrelation feature sets.

The source code for our implementation and experiments is publicly available at <https://github.com/cniel-ud/ICWaves>.

C. Results

We show that the normalizing filters learned display intuitive mapping behaviors. The *Emotion* dataset [8] was collected in the US, and displays a characteristic 60 Hz line noise as seen in Fig. 1. The *Cue* dataset [6] was collected in Europe, and displays a characteristic 50 Hz line noise as seen in Fig. 3; this is an artifact of the two regions’ different electrical regimes. When mapping from the Europe dataset to the US dataset, we can see in Fig. 4 that the filters learned to minimize the 50 Hz spike and introduce a spike at 60 Hz.

As seen in Table I, our results show an improvement compared to no filtering when using *Emotion*-trained classifiers on the *Cue* dataset for labeling ICs using an appropriate CMMN scheme for the classifier. Also unfiltered performance of the BoWaves classifier matches that of ICLabel, indicating that the spatial information in the topographic map feature is not necessary.

The subject-to-subject mapping scheme improves all of the classifier’s performance. For both segment lengths, the subject-to-subject mapping scheme improves the BoWaves performance above the ICLabel benchmark. For classifiers that use the PSD and autocorrelation features, the subject-to-subject mapping scheme improves the brain class F1-score from 0.74 to 0.81 at 5 minutes (+0.07) and from 0.79 to 0.84 at 50 minutes (+0.05).

The performance of the PSD/Autocorrelation classifier was highly dependent on the feature normalization method, particularly for the barycenter mapping schemes. Our initial

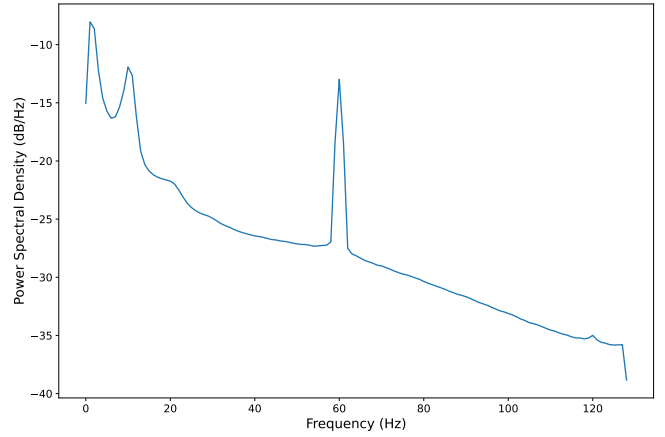


Fig. 2. This is the ℓ_1 -normalized barycenter computed from the source *Emotion* dataset. In the **Barycenter** mapping scheme, all target signals are filtered such that their robust channel-average PSD matches this. Notice the large spike at 60 Hz.

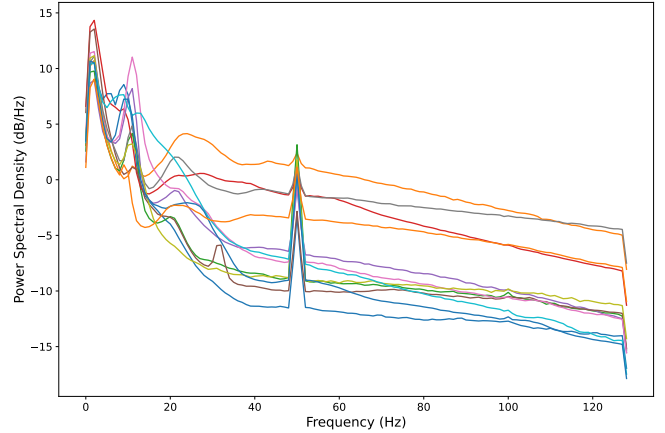


Fig. 3. Here we show the PSD for different subjects in the target *Cue* dataset. Notice the spike at 50 hz.

approach, taken from ICLabel [2], normalized the decibel-scaled PSD by its maximum absolute value. This method proved unsuitable for the ℓ_1 -normalized barycenter CMMN schemes, which uses ℓ_1 -normalized PSDs and thus have a much lower overall signal scale compared to the single-subject PSDs used in the subject-to-subject scheme. To resolve this sensitivity to signal scale, we switched to a more robust min-max normalization that scales features to a 0–1 range (denoted as $\text{PSD}^a/\text{Autocorr.}$ in Table I). This change led to a significant performance increase for the barycenter methods. For instance, with the ℓ_1 -normalized barycenter, the F1-score for 5-minute segments improved from 0.77 to 0.84, demonstrating the effectiveness of CMMN with the corrected feature scaling.

We perform a hypothesis test whether the filtering (subject-to-subject for BoWaves, and normalized barycenter for PSD/Autocorrelation) has a significant improvement in F1 score for the brain-labeled ICs. We use a Wilcoxon rank sign test ($n = 12$, one-sided alternative), and find significant improvements at a level of 0.05 for two of the four cases

TABLE I

F1 SCORE OF BRAIN-LABELED INDEPENDENT COMPONENTS FOR DIFFERENT TEST SEGMENT LENGTHS AND CMMN SCHEMES. BEST PERFORMANCE FOR EACH SEGMENT LENGTH IS BOLDED, AND BEST SCHEME IS UNDERLINED. THE LAST COLUMN CONTAINS THE P-VALUE FOR A ONE-SIDED WILCOXON RANK-SIGN TEST BETWEEN NO FILTERING AND CMMN FILTERED (SUBJECT-TO-SUBJECT FOR BoWAVES, AND NORMALIZED BARYCENTER FOR PSD/AUTOCORR.) ACROSS THE 12 SUBJECTS.

Classifier	Length (minutes)	No filtering	Barycenter	ℓ_1 -Norm. barycenter	Subj-to-subj	p-value
BoWaves	5	0.88 ± 0.05	0.88 ± 0.04	0.87 ± 0.05	<u>0.90 ± 0.08</u>	0.0593
PSD/Autocorr.	5	0.74 ± 0.10	$_{-b}$	0.35 ± 0.30	0.81 ± 0.10	$_{-b}$
PSD ^a /Autocorr.	5	0.77 ± 0.09	0.78 ± 0.12	<u>0.84 ± 0.07</u>	0.79 ± 0.17	0.0046
ICLabel	5	0.88 ± 0.06	N/A ^c	N/A	N/A	N/A
BoWaves	50	0.89 ± 0.09	0.90 ± 0.08	0.88 ± 0.07	<u>0.91 ± 0.08</u>	0.0412
PSD/Autocorr.	50	0.79 ± 0.10	$_{-b}$	0.40 ± 0.28	0.84 ± 0.12	$_{-b}$
PSD ^a /Autocorr.	50	0.83 ± 0.09	0.86 ± 0.09	<u>0.86 ± 0.08</u>	0.85 ± 0.17	0.1696
ICLabel	50	0.89 ± 0.05	N/A	N/A	N/A	N/A

^aUsing 0-1 range normalization rather than max absolute value normalization.

^bAfter noticing the issues with the max absolute value normalization we did not run this case.

^cWe did not apply ICLabel to the CMMN normalized signals, as it was trained over a wide variety of datasets and should be already invariant.

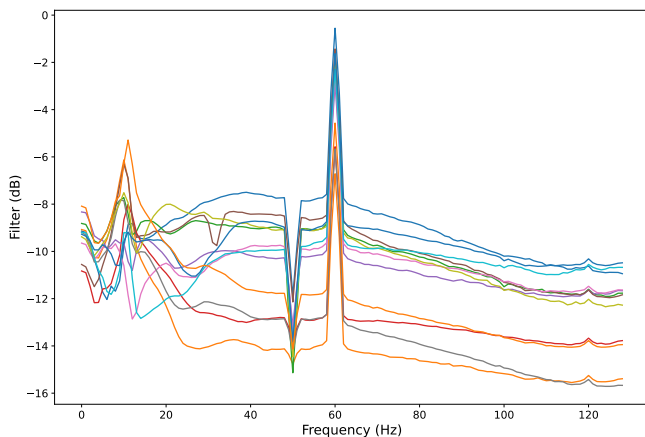


Fig. 4. Here we see the frequency response of filters learned for mapping the *Cue* dataset to the *Emotion* dataset using the **Barycenter** mapping scheme with a normalized barycenter. Notice that the noise at 50 Hz is reduced and the noise at 60 Hz is relatively amplified. Overall, the filter attenuates since the normalized barycenter has lower magnitudes.

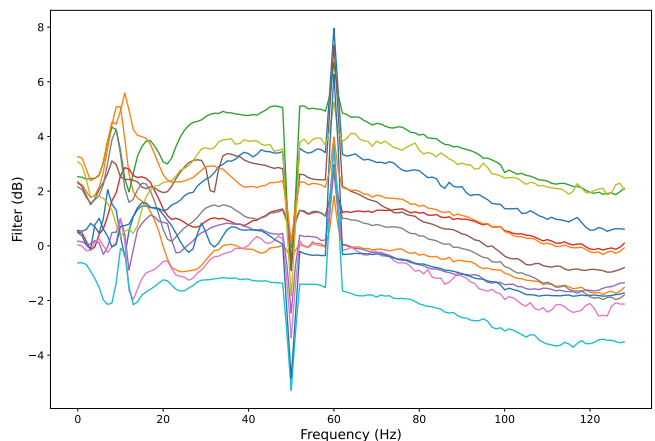


Fig. 5. Similarly to Fig. 4, we see the filters learned for mapping the *Cue* dataset to the *Emotion* dataset, but here they are learned using the **Subj-to-subj** mapping scheme. Even though the mapping scheme is different, the line noises are visibly still being ‘swapped’.

marked in the table.

We can compare these domain adaptation results with the performance on held-out subjects of the source *Emotion* dataset shown in Table II. The BoWaves classifier achieves 0.86 ± 0.10 at 5 minutes and 0.93 ± 0.05 at 50 minutes, and the PSD/Autocorr (with 0-1 range normalization) achieves 0.93 ± 0.05 for 5 minutes and 0.96 ± 0.05 at 50 minutes. The baseline ICLabel achieves 0.88 ± 0.05 at 5 minutes and 0.89 ± 0.07 at 50 minutes. PSD/Autocorr has the best performance at both time lengths, which is in contrast to the worst performance when applied to the new domain; this indicates that PSD/Autocorr overfits to the domain. This highlights both the need for domain adaptation and the generalization ability of the 5-minute BoWaves classifier that has higher F1 in the new domain (0.86 in *Emotion* compared to 0.88 in *Cue* without filtering). It is notable that both classifiers outperform ICLabel given the 50-minute segment on *Emotion*, BoWaves matches the performance of ICLabel on *Cue* without filtering, but only after subject-to-subject

CMMN does the BoWaves outperform ICLabel in *Cue*.

TABLE II

F1 SCORE OF BRAIN-LABELED INDEPENDENT COMPONENTS OF CLASSIFIERS WITHIN DOMAIN ON HELD-OUT SUBJECTS.

Classifier	5 minutes	50 minutes
BoWaves	0.86 ± 0.10	0.93 ± 0.05
PSD/Autocorr. (0-1 range)	0.93 ± 0.05	0.96 ± 0.05
ICLabel	0.88 ± 0.05	0.89 ± 0.07

IV. RELATED WORKS

Domain adaptation is a well-studied problem, with optimal transport methods providing principled approaches [20]. In the context of EEG, recent work [21] uses a geodesic optimization approach to tackle domain adaptation in both the data and label space. Other work [22], [23] use Maximum Mean Discrepancy (MMD) [24] to align source and target EEG data distributions. While MMD is a powerful and general purpose divergence, the Bures-Wasserstein distance

that underlies CMMN is sufficient for zero-mean stationary Gaussian processes.

A clustering-based approach was previously applied [25] to help tackle high variability between subjects. We note that the subject-to-subject and barycenter approaches are two extreme clusterings, and an intermediate clustering could be investigated.

Denoising EEG through independent component analysis is well-known [26], [27] and the automatic labeling of ICs with machine learning has seen a number of advancements [17], [7], [2], [5], [28]. An early method [17] used only six features to reach high levels of inter-expert agreement on labeling of independent components. We note that prior work [7] also classified independent components from the same two datasets [6], [8] that we use, using 65 features. In comparison, BoWaves and PSD/Autocorr use larger number of features characterizing the time-series in terms of its temporal and spectral characteristics. Finally, ICLabel [2] has since become a standard for automatic labeling of independent components; thus, we use it as a benchmark of our classifiers. It is noteworthy that with the proposed CMMN the BoWaves classifier outperforms ICLabel without any access to the spatial information.

V. DISCUSSION

One possible concern is whether channel-averaging is a sufficient characterization of multi-channel EEG given the spectral differences in signals across the scalp. Of course, if the location of the electrodes on the scalp is vastly different such that the spectral content is not comparable, then channel-averaged PSD may not be meaningful, but for EEG montages with whole scalp this should not be an issue.

An interesting extension is to consider domain adaptation for target data collected from EEG montages with limited scalp coverage. In these cases, the channel-averaging in the source should be performed on a subset of channels with the same scalp coverage. Again, as the classifiers tested here only depend on spectral or temporal features, the independent component classifiers will not be limited by the channel coverage. This is because the brain ICs seen during training likely occurred across the brain.

VI. CONCLUSION

In this work we made several key extensions to the recently introduced CMMN methodology [1] to enable domain adaptation of BoWaves classifiers [19], [5], [28] between EEG datasets for independent component classification for artifact removal. We introduce filters defined by channel-averaged PSDs along with a subject-to-subject mapping scheme, and show that our CMMN method results in improvements when classifying brain versus non-brain independent components, achieving domain adaptation between two different datasets with significant differences. With the domain adaptation the BoWaves classifiers exceed the performance of the popular ICLabel [2] classifier. Our method advances the work on EEG artifact-removal across distinct

datasets, an area that is crucial for increasing the clinical utility of EEG recordings.

ACKNOWLEDGMENT

This work was supported in part by the University of Delaware General University Research fund. This research was supported in part through the use of DARWIN computing system: DARWIN – A Resource for Computational and Data-intensive Research at the University of Delaware and in the Delaware Region, which is supported by NSF under Grant Number: 1919839, Rudolf Eigenmann, Benjamin E. Bagozzi, Arthi Jayaraman, William Totten, and Cathy H. Wu, University of Delaware, 2021, URL: <https://udspace.udel.edu/handle/19716/29071>.

The authors thank Laura Frølich, Tobias Andersen, Klaus Gramann, and Morten Mørup for graciously providing access to the *Cue* dataset used for our experiments, and Prof. Gramann for allowing us to post it on OpenNeuro.

REFERENCES

- [1] T. Gnassounou, R. Flamary, and A. Gramfort, "Convolution Monge Mapping Normalization for learning on sleep data," *Advances in Neural Information Processing Systems*, vol. 36, pp. 10457–10476, 2023.
- [2] L. Pion-Tonachini, K. Kreutz-Delgado, and S. Makeig, "ICLabel: An automated electroencephalographic independent component classifier, dataset, and website," *Neuroimage*, vol. 198, pp. 181–197, 2019.
- [3] L. Pion-Tonachini, K. Kreutz-Delgado, and S. Makeig, "The iclabel dataset of electroencephalographic (eeg) independent component (ic) features," *Data in brief*, vol. 25, p. 104101, 2019.
- [4] J. A. Onton and S. Makeig, "High-frequency broadband modulation of electroencephalographic spectra," *Frontiers in human neuroscience*, vol. 3, p. 560, 2009.
- [5] C. H. Mendoza-Cardenas, A. Meek, and A. J. Brockmeier, "Labeling EEG Components with a Bag of Waveforms from Learned Dictionaries," in *ICLR 2023 Workshop on Time Series Representation Learning for Health*, 2023.
- [6] K. Gramann, T. Töllner, and H. J. Müller, "Dimension-based attention modulates early visual processing," *Psychophysiology*, vol. 47, no. 5, pp. 968–978, 2010.
- [7] L. Frølich, T. S. Andersen, and M. Mørup, "Classification of independent components of EEG into multiple artifact classes," *Psychophysiology*, vol. 52, no. 1, pp. 32–45, 2015.
- [8] J. Onton and S. Makeig, *Imagined Emotion Study*. OpenNeuro, 2022.
- [9] H. J. M. Klaus Gramann, Thomas Töllner, "dimension-based attention modulates early visual processing," 2025.
- [10] D. Dowson and B. Landau, "The fréchet distance between multivariate normal distributions," *Journal of multivariate analysis*, vol. 12, no. 3, pp. 450–455, 1982.
- [11] M. Gelbrich, "On a formula for the l2 wasserstein metric between measures on euclidean and hilbert spaces," *Mathematische Nachrichten*, vol. 147, no. 1, pp. 185–203, 1990.
- [12] M. Agueh and G. Carlier, "Barycenters in the wasserstein space," *SIAM Journal on Mathematical Analysis*, vol. 43, no. 2, pp. 904–924, 2011.
- [13] R. Bhatia, T. Jain, and Y. Lim, "On the bures–wasserstein distance between positive definite matrices," *Expositiones mathematicae*, vol. 37, no. 2, pp. 165–191, 2019.
- [14] P. Welch, "The use of fast Fourier transform for the estimation of power spectra: A method based on time averaging over short, modified periodograms," *IEEE Transactions on Audio and Electroacoustics*, vol. 15, pp. 70–73, June 1967.
- [15] P. Virtanen, R. Gommers, T. E. Oliphant, M. Haberland, T. Reddy, D. Cournapeau, E. Burovski, P. Peterson, W. Weckesser, J. Bright, S. J. van der Walt, M. Brett, J. Wilson, K. J. Millman, N. Mayorov, A. R. J. Nelson, E. Jones, R. Kern, E. Larson, C. J. Carey, Í. Polat, Y. Feng, E. W. Moore, J. VanderPlas, D. Laxalde, J. Perktold, R. Cimrman, I. Henriksen, E. A. Quintero, C. R. Harris, A. M. Archibald, A. H. Ribeiro, F. Pedregosa, P. van Mulbregt, and SciPy 1.0 Contributors,

- “SciPy 1.0: Fundamental Algorithms for Scientific Computing in Python,” *Nature Methods*, vol. 17, pp. 261–272, 2020.
- [16] R. Flamary, K. Lounici, and A. Ferrari, “Concentration bounds for linear Monge mapping estimation and optimal transport domain adaptation,” Dec. 2020.
- [17] I. Winkler, S. Haufe, and M. Tangermann, “Automatic classification of artifactual ica-components for artifact removal in eeg signals,” *Behavioral and Brain Functions*, vol. 7, no. 1, p. 30, 2011.
- [18] A. Li, J. Feitelberg, A. P. Saini, R. Höchenberger, and M. Scheltienne, “Mne-icalabel: Automatically annotating ica components with iclabel in python,” *Journal of Open Source Software*, vol. 7, p. 4484, Aug. 2022.
- [19] C. H. Mendoza-Cardenas and A. J. Brockmeier, “Shift-invariant wave-form learning on epileptic ECoG,” in *43rd Annu. Int. Conf. IEEE Eng. Med. Biol. Soc.*, p. 4, aug 2021.
- [20] N. Courty, R. Flamary, D. Tuia, and A. Rakotomamonjy, “Optimal Transport for Domain Adaptation,” *IEEE Transactions on Pattern Analysis and Machine Intelligence*, vol. 39, pp. 1853–1865, Sept. 2017.
- [21] A. Mellot, A. Collas, S. Chevallier, A. Gramfort, and D. A. Engemann, “Geodesic Optimization for Predictive Shift Adaptation on EEG data,” Oct. 2024.
- [22] W. Hang, W. Feng, R. Du, S. Liang, Y. Chen, Q. Wang, and X. Liu, “Cross-Subject EEG Signal Recognition Using Deep Domain Adaptation Network,” *IEEE Access*, vol. 7, pp. 128273–128282, 2019.
- [23] M. Jiménez-Guarneros and P. Gómez-Gil, “Custom Domain Adaptation: A New Method for Cross-Subject, EEG-Based Cognitive Load Recognition,” *IEEE Signal Processing Letters*, vol. 27, pp. 750–754, 2020.
- [24] A. Gretton, K. M. Borgwardt, M. J. Rasch, B. Schölkopf, and A. Smola, “A kernel two-sample test,” *Journal of Machine Learning Research*, vol. 13, no. 25, pp. 723–773, 2012.
- [25] J. Liu, X. Shen, S. Song, and D. Zhang, “Domain Adaptation for Cross-Subject Emotion Recognition by Subject Clustering,” in *2021 10th International IEEE/EMBS Conference on Neural Engineering (NER)*, pp. 904–908, May 2021.
- [26] A. Delorme, T. Sejnowski, and S. Makeig, “Enhanced detection of artifacts in EEG data using higher-order statistics and independent component analysis,” *NeuroImage*, vol. 34, pp. 1443–1449, Feb. 2007. Publisher: Elsevier BV.
- [27] M. Chaumon, D. V. Bishop, and N. A. Busch, “A practical guide to the selection of independent components of the electroencephalogram for artifact correction,” *Journal of Neuroscience Methods*, vol. 250, pp. 47–63, 2015.
- [28] M. I. C. Achuri, M. K. Lara, K. A. Rabbo, B. T. Wilson, A. Meek, J. M. Mahoney, A. E. Hernan, and A. J. Brockmeier, “Interpretable eeg biomarkers for neurological disease models in mice using bag-of-waves classifiers,” *bioRxiv*, pp. 2025–08, 2025.